Clim. Past, 10, 2201–2213, 2014
www.clim-past.net/10/2201/2014/
doi:10.5194/cp-10-2201-2014

Climate of the Past
Open Access

Enhanced 20th-century heat transfer to the Arctic simulated in the context of climate variations over the last millennium

J. H. Jungclaus, K. Lohmann, and D. Zanchettin

Max-Planck-Institut für Meteorologie, Hamburg, Germany

Correspondence to: J. H. Jungclaus (johann.jungclaus@mpimet.mpg.de)

Received: 16 June 2014 – Published in Clim. Past Discuss.: 14 July 2014
Revised: 29 October 2014 – Accepted: 12 November 2014 – Published: 15 December 2014

Abstract. Oceanic heat transport variations, carried by the northward-flowing Atlantic Water, strongly influence Arctic sea-ice distribution, ocean–atmosphere exchanges, and pan-Arctic temperatures. Palaeoceanographic reconstructions from marine sediments near Fram Strait have documented a dramatic increase in Atlantic Water temperatures over the 20th century, unprecedented in the last millennium. Here we present results from Earth system model simulations that reproduce and explain the reconstructed exceptional Atlantic Water warming in Fram Strait in the 20th century in the context of natural variability during the last millennium. The associated increase in ocean heat transfer to the Arctic can be traced back to changes in the ocean circulation in the subpolar North Atlantic. An interplay between a weakening overturning circulation and a strengthening subpolar gyre as a consequence of 20th-century global warming is identified as the driving mechanism for the pronounced warming along the Atlantic Water path toward the Arctic. Simulations covering the late Holocene provide a reference frame that allows us to conclude that the changes during the last century are unprecedented in the last 1150 years and that they cannot be explained by internal variability or natural forcing alone.

1 Introduction

The Arctic is one of the regions where climate change has been diagnosed most drastically in terms of warming and sea-ice decline over the last decades. Direct temperature measurements are, however, scarce and only available for the last century. Reliable observations of sea-ice evolution are even more limited, covering only the satellite era. On decadal timescales, internal variations can substantially contribute to Arctic climate variability (Bengtsson et al., 2004; Beitsch et al., 2014), and the relative role of external drivers is still under debate (Booth et al., 2012; Zhang et al., 2013). High-resolution reconstructions of palaeoclimatic variables over the late Holocene provide a reference frame and put recent changes in context with long-term natural variations. Ongoing efforts, such as the Past Global Changes 2K network (PAGES2K; Ahmed and PAGES 2k Consortium, 2013) initiative, provide regional syntheses of reconstructions that can be compared with model simulations. While most of the PAGES2K reconstructions rely on terrestrial proxies, high-quality marine palaeodata become increasingly available at annual to decadal resolution. Novel proxies have been developed to reconstruct, for example, dynamical quantities such as near-bottom flow strength in the Nordic Seas overflow regions (e.g. Boessenkool et al., 2007). Of particular value are reconstructions from key locations, such as major conduits of the large-scale ocean circulation. Spielhagen et al. (2011) and Dylmer et al. (2013) have published records from marine sediments off Svalbard that reflect temperature changes in the Atlantic Water (AW) in Fram Strait over the last 2000–3000 years. The time series show centennial-scale modulations of the AW temperatures and, as a pronounced common feature, a dramatic, unprecedented warming over the 20th century. The authors speculate that the observed warming reflect considerable changes in the lateral heat transfer to the Arctic that might have contributed to the rapid warming and sea-ice decrease during the 20th century.

Earth system model (ESM) simulations over the last millennium provide a tool to test such hypotheses, and to investigate the relative role of internal variability on the one hand and natural and anthropogenic forcing on the other hand. Provided that the model adequately simulates regional-scale fea-

tures, simulations also allow for attributing locally observed variations to changes in large-scale dynamics. In general, the model results have to be confronted with observations and reconstructions to assess to what extent they reproduce the real climate evolution, both in direct comparison (e.g. Fernández-Donado et al., 2012) and in a statistical sense (Bothe et al., 2013). In this paper, we use the results of Max Planck Institute Earth System Model (MPI-ESM) simulations for the last millennium and the industrial period to address the following research questions:

1. Can the simulations reproduce important features of reconstructed climate indicators in high northern latitudes during the last millennium and in the 20th century, both on a continental and local scale?

2. How exceptional is the observed 20th-century AW warming in Fram Strait in the context of the climate evolution during the last millennium, and what implications does it have for the heat transfer to the Arctic?

3. What are the mechanisms behind the observed and reconstructed changes?

Regarding the latter, we concentrate in this paper on the 20th-century changes in high northern latitudes and the North Atlantic and devote a subsequent study to pre-industrial variations and their relation to external forcing. The paper is organized as follows. In Sect. 2, we describe the MPI-ESM model set-up and the boundary conditions applied for the simulations covering the last millennium. Results for integrated high-northern-latitude changes and the evolution of the Atlantic Water transfer from the North Atlantic to the Arctic are given in Sect. 3. In Sect. 4, we formulate a dynamical interpretation of the results and discuss implications for 20th-century climate change in the North Atlantic realm in Sect. 5. Main conclusions are given in Sect. 6.

2 The model system and the experimental design of the last-millennium simulations

The model employed in this study is the Max Planck Institute Earth System Model. MPI-ESM and its various configurations contributing to the Coupled Model Intercomparison Project, phase 5 (CMIP5), have been documented in a special issue of the Journal for Advances in Modeling Earth Systems (JAMES). The configuration for palaeo-applications (MPI-ESM-P) used here is identical to the low-resolution configuration (MPI-ESM-LR) described in the JAMES publications by Giorgetta et al. (2013) and Jungclaus et al. (2013) with two exceptions: first, the dynamic vegetation module is switched off in order to allow for the implementation of land-cover change maps (Pongratz et al., 2008) as in the earlier, lower-resolution model version described by Jungclaus et al. (2010). Second, the orbital forcing is prescribed by a table providing annual values for eccentricity, obliquity, and perihelion, whereas the LR version uses a calendar-based orbit. The atmosphere model ECHAM6 (Stevens et al., 2013) is run at a horizontal resolution of spectral truncation T63 (1.875°) and 47 vertical levels, resolving the stratosphere up to 0.01 hPa. The ocean/sea-ice model MPIOM (Max Planck Institute Ocean Model; Marsland et al., 2003; Jungclaus et al., 2013) features a conformal mapping grid with nominal 1.5° resolution and 40 vertical levels (GR1.5L40). It is noteworthy for our study that the GR1.5L40 grid possesses one grid pole over Antarctica and one grid pole over Greenland, which leads to considerably higher resolution in the regions of interest for this study, i.e. the northern North Atlantic (Jungclaus et al., 2008). In Fram Strait, for example, the grid size in cross-channel direction is about 30–40 km. The simulations over the last millennium (past1000) follow the protocol of the Paleoclimate Modelling Intercomparison Project, phase 3 (PMIP3). As part of this protocol, Schmidt et al. (2011) summarize different choices for external forcing and boundary conditions and provide tables for well-mixed greenhouse gases (CO_2, CH_4, N_2O) and orbital parameters. In contrast to the millennium simulations described in Jungclaus et al. (2010), which featured an interactive carbon cycle and prognostic CO_2, we use prescribed CO_2 in the past1000 runs analysed here. We employed the Crowley and Unterman (2013) reconstruction for volcanic aerosol optical depth and effective radius and the Pongratz et al. (2008) reconstruction of global land-cover and agricultural areas. For solar radiation we have followed the approach described in Schmidt et al. (2011) combining the Vieira et al. (2011) total solar irradiance (TSI) reconstruction over the Holocene with the Wang et al. (2005) data set that provides the recommended solar forcing for the CMIP5 20th-century (1850–2005) simulations. An artificial 11 yr cycle of varying amplitude is imposed over the pre-industrial period (see Schmidt et al., 2011, for details). Linear interpolation was used to calculate monthly TSI averages from the reconstructed annual TSI values for the period 850–1849 scaled to Total Irradiance Monitor (TIM) data, except for the flux at 180.5 nm. Spectral solar irradiance (SSI) for the 14 short-wave spectral bands of ECHAM6's radiation scheme was calculated so that the sum of SSI yields TSI. Energy in the part of the spectrum below the shortest wavelength of the radiation scheme (200 nm) and above the longest (12 195.1 nm) was added to the first and last band, respectively. Monthly average ozone concentrations for the period 850–1849 are calculated using the 1850–1860 monthly climatology of ozone concentrations from the AC&C/SPARC Ozone Database as a basis and representing the ozone dependency on solar irradiance through regression coefficients between historical ozone concentrations and the annual 180.5 nm solar flux. An 1155-year-long pre-industrial control integration (PiCtrl) under fixed 1850 boundary conditions serves as a reference simulation for forced experiments. To conduct the past1000 simulations, we first ran a 400-year-long adaptation simulation starting from the end of piCtrl to adjust to 850 boundary conditions and thereafter

started the three realizations past1000-r1, past1000-r2, and past1000-r3. The past1000-r1 and past1000-r2 experiments were initialized with the same ocean state, but they differ in the standard deviation of the assumed lognormal distribution of the volcanic aerosol size (1.2 µm in r1, 1.8 µm in r2 and r3). The simulations past1000-r2 and past1000-r3 used the same parameter setting but were started from different initial conditions. Furthermore, ozone concentration data used in past1000-r1 are affected by use of a 1-month-shifted annual cycle in the AC&C/SPARC ozone climatology, an issue solved in past1000-r2 and past1000-r3. While the three simulations are therefore not an ensemble of three runs carried out with an identical model and forcing/boundary conditions, we consider the effect of the different setting small enough to regard the runs as three realizations of possible last-millennium climate evolution under parameter and forcing uncertainties. The PMIP3 protocol defines the past1000 integration period as 850–1849. To relate the recent climate evolution to the late-Holocene variability, we continued the respective past1000 simulations over the historical period (1850–2005). The applied boundary conditions follow the CMIP5 protocol, except for land-cover-changes, where we continue the simulations with the Pongratz et al. (2008) data set. In the following, we refer to the combined past1000 and historical simulations covering the period 850–2005 as pr1, pr2, and pr3. Since the emphasis of our present study is on the 20th-century changes, we also include in some analyses in Sects. 4 and 5 one additional MPI-ESM-P "historical" (hr1) simulation (1850–2005), which was initialized from the PiCtrl experiment.

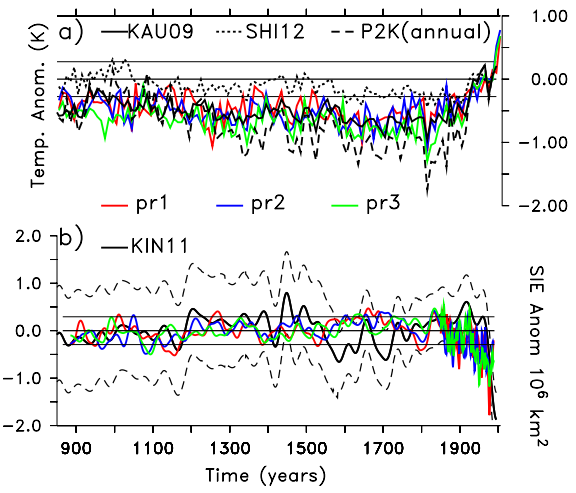

Figure 1. Simulated time series (coloured lines for experiments pr1, pr2, pr3) of high-northern-latitude climate variables in comparison with reconstructions (black lines): **(a)** 10-year averages of Arctic summer (JJA) surface air temperatures as anomalies w.r.t. the 1960–1990 mean. Summer temperature reconstructions are from (solid black) Kaufman et al. (2009) and (dotted black) Shi et al. (2012). The PAGES2K reconstruction representing annual temperatures is also shown (dashed black). **(b)** Late-summer (August) sea-ice extent (in 10^6 km^2) as anomalies w.r.t. the pre-industrial mean in comparison with the reconstruction by Kinnard et al. (2011): the thick black line denotes the 40-year smoothed reconstruction, the dashed black lines their 95 % confidence interval; for the simulations, a 41-year running mean was applied for pre-industrial millennium and a 5-year running mean for 1850–2005 to better display 20th-century variability. Thin horizontal lines bracketing the zero line in **(a)** and **(b)** indicate the respective 2σ ranges derived from the 1000-year-long PiCtrl experiment.

3 Last-millennium evolution of high-northern-latitude climate

3.1 Pan-Arctic temperature and sea-ice extent

We start the analyses with quantities that reflect the general climate evolution in high northern latitudes. Reconstructing regional-scale temperature and other climate variables such as sea-ice extent in sparsely sampled areas is still challenging. Only recently have pan-Arctic reconstructions for temperature been published (Kaufman et al., 2009; Shi et al., 2012), mostly based on terrestrial proxies (tree rings) and ice cores. The PAGES2K consortium reviewed reconstruction data and methods and constructed seven continental-scale temperature records, including the Arctic (Ahmed and PAGES 2k Consortium, 2013). The reconstructed temperature records (black lines in Fig. 1a) have in common that they show a gradual cooling during the last millennium, possibly reflecting the overall evolution from a warmer Medieval Warm Period (MWP) to an anomalously cold Little Ice Age (LIA). Note that the PAGES2K record reflects annual mean temperatures whereas the other two represent the summer season. All reconstructions (and the instrumental data that they are matched to) show a strongly reversed trend during the 20th century. The Shi et al. (2012) and Kaufman et al. (2009) summer temperature reconstructions disagree on the magnitude of the pre-industrial cooling. This reflects differences in the proxies chosen, their geographical distribution, and the statistical methods used to match the proxies to historical observations. We are not in a position to judge which of the two time series reflects more appropriately the real climate evolution; we therefore regard the discrepancy as a measure of uncertainty in reconstructed climate. The simulated summer temperatures are compatible with the reconstructions and match closely the Kaufman et al. (2009) data. Individual simulations (coloured lines in Fig. 1a) show relatively strong fluctuations and ensemble realizations differ often quite strongly (about 0.5 °C) for a given period. In contrast to global and hemispheric averages (not shown here, but see Fig. 5 in Jungclaus et al., 2010), individual volcanic eruptions (like the very strong 1258 or 1453 tropical eruption) or clusters of volcanic events are not clearly discernible, with the exception of the 1809 and 1815 (Tambora) eruptions, where all simulations show a similar cold excursion,

in accordance with the Kaufman and Past2K reconstructions. The resilience to volcanic forcing reflects the relatively small signal-to-noise ratio of Arctic summer temperatures, due to both strong internal variability of the Arctic regional climate (e.g. Beitsch et al., 2014) and seasonal character of local response mechanisms, which are most prominent in boreal winter (e.g. Zanchettin et al., 2012). Zanchettin et al. (2013) have also highlighted the role of background conditions (e.g. during the closely following 1809 and 1815 eruptions) for the actual response patterns, in particular at high latitudes. The Arctic warming throughout the 20th century is also well reflected in the model simulations, and the pronounced variations such as the warm phase in the first half of the last century are well within the ensemble range of the historical experiments.

The summer sea-ice reconstruction by Kinnard et al. (2011) comes with a relatively large range of uncertainty (dashed black lines in Fig. 1b), but the main characteristic is that of a mirror image of the pan-Arctic surface temperature evolution: a gradual increase in sea-ice extent during the pre-industrial millennium is replaced by a drastic decline in the 20th century (Fig. 1b). The decline of sea-ice extent sets in, however, more abruptly in the mid-20th century in contrast to the relatively gradual warming. The past1000 simulations reproduce a similar long-term trend over the pre-industrial millennium, and the 20th-century simulations terminate at an extent that is equally as low as the observations. In the simulations, the sea-ice decline begins, however, earlier featuring a temporal evolution more similar to the pan-Arctic temperature (Fig. 1a). In fact, all four historical simulations show ice extent anomalies below the reconstruction's mean estimate between 1870 and 1950. The sea-ice reconstruction exhibits a pronounced relative minimum in the late 16th century, which none of the three past1000 simulations reproduces. Notwithstanding questions regarding uncertainties in the reconstructions, it is difficult to relate the event to known volcanic or solar forcing variations (e.g. the minimum around 1700 appears at the time of the Maunder Minimum in solar variations). The anomalies in the 15th to 17th century exceed the 2σ range of control experiment variability significantly. We have detected events of similar magnitude in unforced control simulations, but they appear only rarely (once in a 1000 yr simulation). It is therefore possible that the model underestimates internal variability of the sea-ice extent.

3.2 Fram Strait Atlantic Water temperatures

The reconstructions of AW temperatures stem from a marine core at site MSM5/5-712 at 78°54.94′ N, 6°46.04′ E (see Spielhagen et al., 2011, and Werner et al., 2011 for details). The authors provide two temperature records, one based on a modern analogue technique (SIMMAX), and one based on the magnesium / calcium (Mg / Ca) ratio of *Neogloboquadrina pachyderma*. Habitat and plankton bloom estimates indicate that both proxies reflect mid-summer conditions in the upper part of the AW layer. During pre-industrial times, the Mg / Ca-derived record exhibits much stronger variability, which might reflect inaccuracies in recording the cold-water range (Spielhagen et al., 2011). Both reconstructions, however, fluctuate around very similar pre-industrial mean values (3.4 and 3.6 °C) and indicate a warming of roughly 2 °C during the 20th century (Fig. 2). A similar temperature increase is also found in continued measurements from Svalbard fjords from 1912 to 2005 (Pavlov et al., 2013) and agrees with previous estimates of 20th-century evolution of AW properties in the northern North Atlantic (Polyakov et al., 2004). Another late-Holocene sedimentary record from Malangen Fjord in northern Norway (Hald et al., 2011) reflects local variations in the influx of AW and shows a similar temperature evolution over the last 1200 years, including an unprecedented warming in modern times.

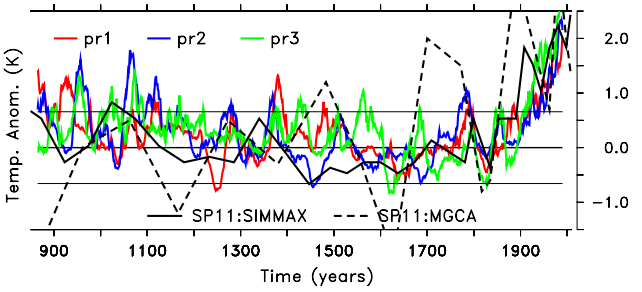

Figure 2. Simulated time series (coloured lines for experiments pr1, pr2, pr3) of Atlantic Water temperature anomalies w.r.t. the pre-industrial mean in Fram Strait (78° N, 50 m depth) in comparison with the reconstruction by Spielhagen et al. (2011) obtained by the (solid black) SIMMAX and (dashed black) Mg / Ca methods. The thin horizontal lines bracketing the zero line indicate the respective 2σ ranges derived from the 1000-year-long PiCtrl experiment.

We compare the Spielhagen et al. (2011) reconstructions with simulated fluctuations of temperatures in the AW core at 50 m depth in Fram Strait at about 78° N (Fig. 2). The relatively low temporal resolution and the strong fluctuations in the Mg / Ca record prohibit a very detailed comparison in the pre-industrial millennium. The simulations and the SIMMAX data agree on a change from slightly warmer-than-average temperatures in the first centuries to colder conditions in the 16th to 18th centuries, reflecting the general change from MWP to LIA conditions. Interestingly, all time series show a cold spell in the early 19th century, likely recording the 1809 and 1815 eruptions. During the 20th century, simulations and the SIMMAX record agree on a 2 °C warming. The simulations also exhibit considerable decadal to multidecadal variations that are not covered or sub-sampled by the reconstructions' resolution. The ensemble spread and the relatively large variability range obtained from the unforced control run (Fig. 2) point to a large fraction of internal variability.

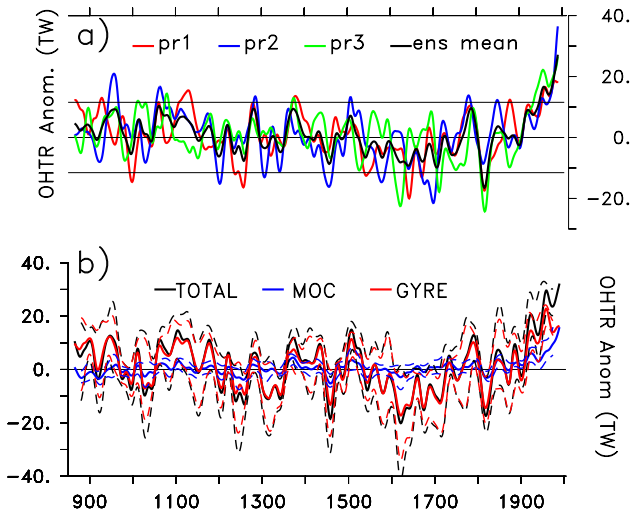

Figure 3. (a) Simulated ocean heat transport (OHTR) to the Arctic (combined OHTR through Fram Strait and Barents Sea Opening) as anomalies w.r.t. the pre-industrial mean; coloured lines indicate individual simulations pr1, pr2 and pr3, and the solid black line is the ensemble mean; thin horizontal lines bracketing the zero line indicate the respective 2σ ranges derived from the 1000-year-long PiCtrl experiment. **(b)** Total OHTR (black lines, TOHTR) averaged over 60–65° N, subdivided into gyre-related OHTR (red, GOHTR), and overturning-circulation-related OHTR (blue, MOHTR). Thick lines represent the ensemble means, and the dashed lines the respective ensemble ranges. All time series were smoothed by a 31-year running mean. Units are TW ($1\,\mathrm{TW} = 10^{12}$ Watt).

Clearly, the warming in the industrial period exceeds the 2σ range of the undisturbed simulation. Spielhagen et al. (2011) speculate that the diagnosed warming infers a considerable increase in heat transfer to the Arctic. In the model simulations, we can quantify the heat flux changes and display in Fig. 3a the combined total ocean heat transport (TOHTR) through Fram Strait and through the Barents Sea Opening (BSO), which both show the unprecedented increase in the 20th century. Firstly, we confirm that the AW temperature record indeed reflects changes in heat transfer through the most important conduits towards the Arctic. The correlation coefficients between AW temperatures and TOHTR (smoothed by a 31 year running mean) exceed 0.9 at zero time-lag in all three past1000 simulations. Simulated TOHTR anomalies are shown with respect to (w.r.t.) the pre-industrial (850–1849) mean of about 80 TW ($1\,\mathrm{TW} = 10^{12}$ Watt). The simulated transports are compatible with observations indicating a heat transport of 30–40 TW in Fram Strait (Schauer et al., 2008) and 30–76 TW in BSO (Årthun et al., 2012). Observations of heat transports are, however, only available for the most recent decades and may be influenced by decadal-scale variability as well. During the pre-industrial period, there are TOHTR fluctuations of the order of 10–20 TW, and the ensemble indicates somewhat higher-than-normal TOHTR in the early part of the simulation and less TOHTR in the 16th and 17th century. Large volcanic eruptions (1258, 1453, and 1815) leave an imprint on the heat transports leading to reduction of heat transfer to the Arctic (Zanchettin et al., 2012). The most pronounced feature of our smoothed time series from the simulations is, however, a consistent increase of up to 30 TW during the 20th century, reflecting a 40 % increase over the pre-industrial mean.

The modulation of the AW temperature could either be driven by local changes in the wind system (Bengtsson et al., 2004) or be part of variations in the warm-water path associated with the North Atlantic Current or the Atlantic Meridional Overturning Circulation (AMOC), as has been suggested, for example, by Polyakov et al. (2004). However, recently Lozier (2010) and Lozier et al. (2010) have demonstrated that overturning and gyre circulation in the North Atlantic are strongly linked and that the image of a continuous conveyor belt associated with the AMOC may be misleading. Building on earlier results analysing Arctic warming events in an unperturbed control integration (Beitsch et al., 2014), we therefore decompose the TOHTR in the Atlantic Basin into its overturning and gyre components (MOHTR and GOHTR, respectively). The first reflects the zonal average heat transport, the second the deviations of the zonal average (e.g. Eden and Jung, 2001; Drijfhout and Hazeleger, 2006). First, we calculate the correlations between the TOHTR at the entrance to the Arctic (Fig. 3a) and the components of the basin-scale OHTRs for all latitudes. High correlations are found in particular in the subpolar North Atlantic between GOHTR and heat transfer to the Arctic (not shown). At the entrance to the Nordic Seas at 60–65° N (Fig. 3b) we can see that most of the modulation in the heat transfer to the Arctic during the millennium can be traced back to downstream fluctuations in GOHTR. The gyre heat transport features multi-centennial changes from stronger-than-normal conditions in the early centuries of the simulation to weaker conditions during the Little Ice Age. The 20th century stands out again with its unprecedented increase in the TOHTR. Most of the increase at 60–65° N is carried by an increase in the gyre component, but, interestingly, the overturning component also shows a clear positive trend over the 20th century and apparently contributes to high-latitude warming despite the fact that AMOC decreases at 30° N over the 20th century.

4 Origin of the 20th-century heat transfer increase

In the following, we focus on the changes in the 20th century and elucidate the relation between heat transfer changes in Fram Strait and the subpolar North Atlantic. We consider simulated linear 100 years trends (1905–2005) and compare them with the expected range of internal variability as expressed in the 5th–95th-percentile range of the respective variables taken from the 1000-year-long PiCtrl simulation.

The changes in the heat transport components over the 20th century reflect trends in the large-scale ocean circula-

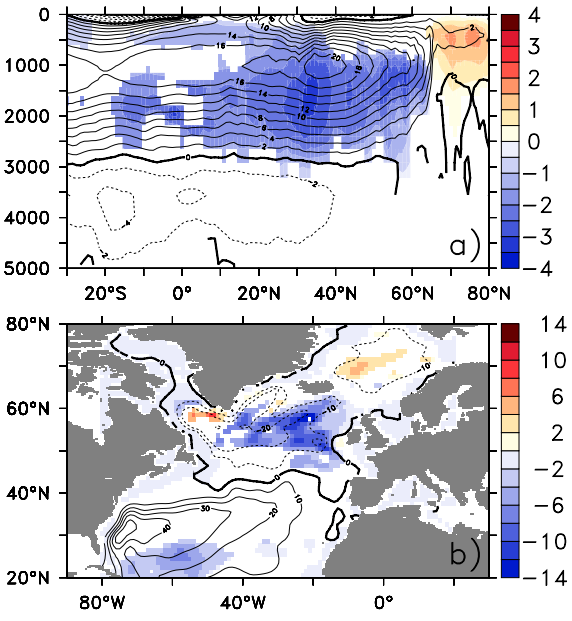

Figure 4. Simulated 20th-century linear trends (1905–2005) in the pr2 simulation (colour shading) of **(a)** meridional overturning circulation and **(b)** barotropic stream function in the North Atlantic. Units are sverdrups ($1\,\mathrm{Sv} = 10^6\,\mathrm{m}^3\,\mathrm{s}^{-1}$) per 100 years. Contour lines (contour intervals 2 Sv for overturning and 10 Sv for barotropic stream function) describe the pre-industrial mean state. In both panels, only anomalies are shown that exceed the 5th–95th-percentile range of centennial trends derived from the PiCtrl simulations.

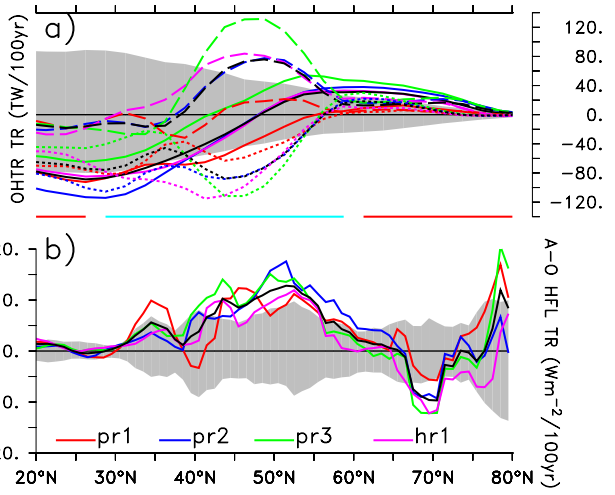

Figure 5. Simulated 20th-century linear trends (1905–2005) as zonal averages over the Atlantic Basin (experiments pr1, pr2, pr3, and hr1 as indicated by coloured lines; black lines indicate ensemble means): **(a)** (solid lines) TOHTR, (dashed lines) GOHTR, and (dotted lines) MOHTR. Light-blue and red horizontal lines at the bottom of the plot indicate regions where the ensemble-mean TOHTR divergence is positive (cooling by lateral advection: light-blue) or negative (warming by lateral advection: red). **(b)** Atmosphere–ocean heat fluxes. Positive values indicate increased heat transfer from the atmosphere to the ocean or cooling of the atmosphere by the ocean. Coloured lines are individual simulations, and the black line is the ensemble mean. In **(a)** and **(b)**, the grey-shaded regions indicate the 5th–95th-percentile ranges of centennial trends in the unperturbed PiCtrl experiment.

tion. Figure 4 shows the centennial trends for the AMOC stream function (Fig. 4a) as function of latitude and for the barotropic horizontal stream function (Fig. 4b) together with their long-term means. The AMOC increases at higher latitudes, but the most prominent feature is a broad-scale weakening in subtropical and subpolar latitudes at depth below 1000 m. As has been described in previous studies (e.g. Latif et al., 2006), this weakening is associated with reduced deep-water formation, most prominently in the Labrador Sea (see below). On the other hand, the circulation cell reaching into the Nordic Seas strengthens as more overturning occurs at higher latitudes. The barotropic stream function trends are characterized mainly by a pronounced strengthening (the negative sign refers to more cyclonic circulation) in the central and eastern part of the subpolar basin. In the central Labrador Sea, the gyre circulation weakens, which is, again, compatible with reduced deep-water formation in the main convection region. There is also indication of a weakening of the gyre circulation in the Nordic Seas.

The change in TOHTR in the Atlantic Basin reflects the trends in its components: in particular in subpolar latitudes, a weaker overturning component is mostly compensated by a stronger gyre component (Fig. 5a), but the resulting TOHTR does not exceed the range of internal variability. North of 55° N, changes in both components are much smaller but constructively add up to positive TOHTR trends. The trends are robust in the four simulations, and the 20th-century TOHTR trends exceed the 5–95 % range deduced from the PiCtrl run in three of the four simulations. In subtropical latitudes, overturning transports are also smaller, but they are not compensated by the gyre transports. Thus the TOHTR here are considerably weaker and exceed the 5–95 % range of trends in the control simulation. Meridional divergence or convergence of TOHTR then causes regional cooling or warming, if not compensated by surface heat fluxes. Therefore, positive slopes of the TOHTR curves in Fig. 5a indicate cooling, while negative slope indicate warming, as indicated by the red and light-blue horizontal lines at the bottom of Fig. 5a. Regions where divergence of advective lateral heat transport cools the ocean (Fig. 5a) are associated with positive atmosphere-ocean heat flux trends, indicating that the colder ocean is cooling the atmosphere. Hence the atmosphere is damping the ocean-induced changes rather than enforcing them. Trends in the upper-ocean temperatures are negative roughly between 45 and 60° N, and, since they are only partly compensated by freshening (not shown), there are considerable changes in the density structure, as is shown for the pr2 experiment in Fig. 6 (results are similar for all simula-

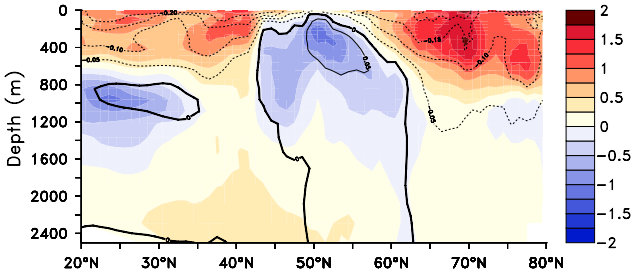

Figure 6. Simulated 20th-century linear trends (1905–2005) as zonal averages over the Atlantic Basin for potential temperature (colour shading) and density (contours, contour interval 0.05 kg m^{-3}) trends from the pr2 experiment.

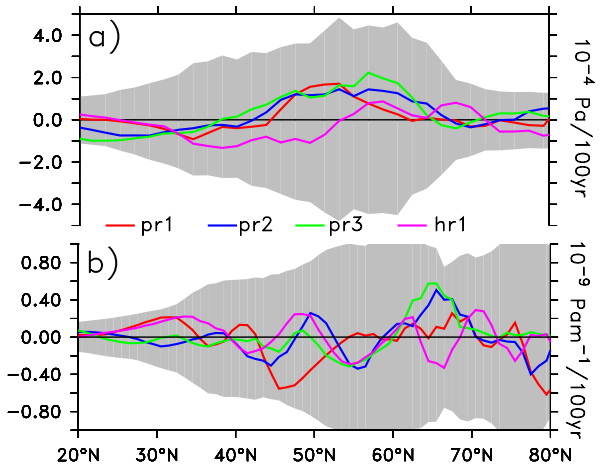

Figure 7. Simulated (experiments pr1, pr2, pr3, and hr1) 20th century linear trends (1905–2005) as zonal averages over the Atlantic basin of **(a)** zonal wind stress (units 10^{-4} Pa / 100 years) and **(b)** wind stress curl (in 10^{-9} Pa / 100 years). Coloured lines denote the experiments pr1, pr2, pr3, and hr1, and the grey-shaded regions bracketing the zero line show the 5th–95th-percentile range of centennial trends in the unperturbed PiCtrl experiment.

tions). Increased density in the centre and more pronounced doming of the subpolar isopycnals is typical for a strengthening gyre. The increasing horizontal density gradients, on the other hand, indicate higher baroclinic pressure gradients and further accelerate the gyre (Greatbatch et al., 1991; Levermann and Born, 2007).

A possible reason for the acceleration of the gyre circulation could be changes in the wind system. Modulations of large-scale atmospheric pressure patterns like the North Atlantic Oscillation or the East Atlantic Pattern leave their specific imprint on the wind-driven ocean circulation (Häkkinen and Rhines, 2009) and may be important also on centennial timescales (e.g. Sedláček and Mysak, 2009). In particular, the gyre would respond to changes in the wind-stress curl caused, for example, by a poleward shift of the westerlies due to global warming (e.g. Saenko et al., 2005). The centennial trends in the zonal wind stress component are indeed relatively coherent in the past1000 experiments and resemble those obtained by Saenko et al. (2005) in idealized CO_2-doubling experiments: stronger positive wind stress north of 40° N and slightly negative values in the subtropical region (Fig. 7a). While they are consistent in three of the four experiments considered here, the changes are well within the 5th–95th-percentile range obtained from the unperturbed control experiment. Moreover, trends in wind-stress curl (Fig. 7b) indicate coherent changes only in the Southern Hemisphere (not shown), which is, again, consistent with the findings by Saenko et al. (2005), who applied somewhat stronger CO_2 forcing.

To further elucidate the origin of the circulation changes, we identify first the reason for the weakening of the AMOC in the subtropical and subpolar North Atlantic. A key ingredient modulating the AMOC here is the strength of deep-water formation in the Labrador Sea (Latif et al., 2006; Lohmann et al., 2014). To quantify the latter, we calculate the thickness of the Labrador Sea Water (LSW) in the region (for details, see Lohmann et al., 2014). Normalizing the anomalies, we see a clear co-variability with the AMOC at 30° N and 1500 m depth when AMOC lags by roughly 8–10 years. Next, we establish a link between LSW thickness and surface properties by correlating LSW thickness with the surface density field (not shown), which reveals the central Labrador Sea as convection hot spot. The evolution of surface density, temperature, and salinity in the so-identified region reveals, as expected, that enhanced LSW formation comes together with positive density anomalies at the surface that reduce the static stability and induce convection. Also shown in Fig. 8a are the corresponding temperature and salinity time series. Following the evolution through the last 3 centuries indicates pronounced multidecadal variability and pronounced differences between the industrial period and the centuries before. The multidecadal variability is characterized by co-varying temperature and salinity, where apparently density is determined by the salinity changes (e.g. fresher and lighter conditions lead to less dense surface waters, which are not compensated by colder temperatures). The variations in the regional freshwater budget are mainly caused by modulations of the sea-ice and freshwater supply from higher latitudes (Jungclaus et al., 2005) and from redistribution of zonal salinity transport by the Irminger Current. During the 20th century, however, this relation breaks down as somewhat fresher conditions (also caused by increasing sea-ice and freshwater export through Denmark Strait, not shown) go along with a general warming, partly caused by direct radiative forcing, partly be redistribution of heat by an enhanced Irminger Current. As a result, AMOC weakens at latitudes downstream from the LSW formation region. The temporal evolution of the vertical density structure in the Labrador Sea indicates then generally less dense conditions in the upper 2000 m. Interestingly, the deepest layers are characterized by relatively colder temperatures and higher densities that are caused by the enhanced

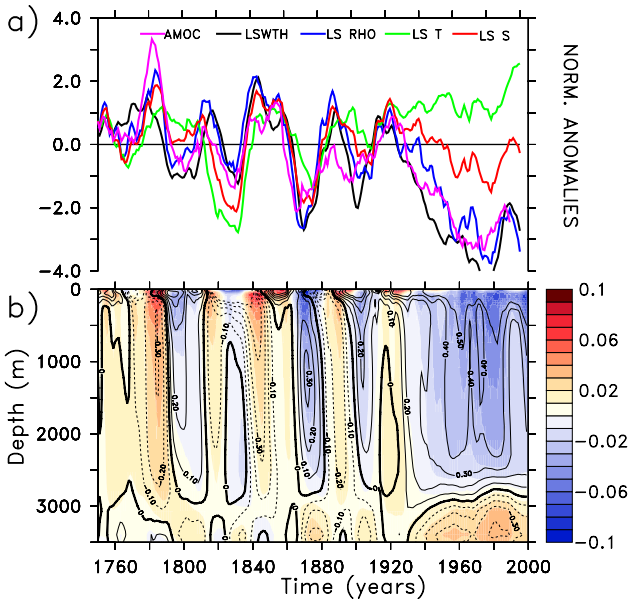

Figure 8. (a) Evolution of the Labrador Sea Water thickness (LSWTH, defined as the depth difference between the isopycnals $\sigma_2 = 36.74$ and $\sigma_2 = 36.82$, averaged over 60–45° W, 50–60° N), AMOC stream function at 30° N and 1500 m depth (displayed here with a 10-year time-lag), and surface water mass properties in the region where convection takes place in the Labrador Sea: density (LS RHO), temperature (LS T), and salinity (LS S). All time series are smoothed using an 11-year running mean and are shown as normalized anomalies w.r.t. the pre-industrial means. **(b)** Evolution of potential density (colour shading) and potential temperature (contours, contour intervals 0.05 K) as function of depth and time for the Labrador Sea in the pr2 simulation. An 11-year running mean was applied to the data.

overturning in the Nordic Seas and associated changes in the strength and density of the Denmark Strait overflow. Changes in the vertical density structure not only are important for the east–west density gradient driving the AMOC (Lozier et al., 2010), but they also affect the baroclinic structure of the gyre directly (Drijfhout and Hazeleger, 2006).

5 Discussion

Our analysis has demonstrated that the increasing heat transports to higher latitudes are mainly caused by changes in the gyre and overturning circulation in the subpolar North Atlantic. These changes are caused by a reduction in deep-water formation in the Labrador Sea, which leads to reduced overturning circulation in subtropical and subpolar latitudes. In addition, changes in the vertical structure of water masses at the western boundary can modify the baroclinic gyre circulation (Drijfhout and Hazeleger, 2006). The associated changes in MOHTR and GOHTR lead to enhanced TOHTR towards higher latitudes and heat transport divergence (cooling) in the subpolar region. The colder and denser Subpolar Gyre (SPG) then spins up baroclinically, which further increases the GOHTR (dashed lines in Fig. 5a), which, in turn, extracts even more heat from the SPG centre and further increases the horizontal density gradient. Thus a positive feedback mechanism is initiated. The mechanism can be compared to the one described by Levermann and Born (2007) and Born et al. (2013a). These authors describe a positive feedback, where an (somehow) accelerated gyre leads to increasing east–west temperature and salt transports along its northern rim. Increasing salinity then leads to denser surface waters in the Labrador Sea and to enhanced convective activity, which further spins up the gyre. In our simulations, we see also a redistribution of salinity during the 20th century change in gyre circulation resulting in higher salinities in the western part of the basin. However, in contrast to the mechanism described by Levermann and Born (2007), the positive temperature anomalies dominate the near-surface density evolution in the industrial period and Labrador Sea convection rather decreases. Levermann and Born (2007) demonstrated that a bistability regime exists where the transition between the two regimes can be triggered by small fluctuations in surface freshwater flux. Born et al. (2013a) extended the study and found multiple circulation modes in PiCtrl experiments in 6 out of 19 models (among them MPI-ESM-LR). Even though we find some differences to their mechanism, it is possible that the relatively strong response of the SPG is an expression of such a transition, here triggered by changes in the AMOC. The wind-stress changes may also (Fig. 7) play a role in initiating the change in the gyre circulation by modified Ekman and/or Sverdrup transports. Furthermore, gyre circulation changes can also directly be driven by changes in the baroclinic structure at the western boundary, as has been shown in the global warming simulations by Drijfhout and Hazeleger (2006). At the western boundary near the exit of the Labrador Sea (Fig. 8b), the density changes are consistent with a weakening of Labrador Sea Water production and an increase in overflow-derived density, similar to what has been found by Drijfhout and Hazeleger (2006). It is difficult, however, to exactly detect which component is more important in initially triggering the mechanism. For this, additional sensitivity experiments (e.g. partial-coupling experiments) would be necessary, which is beyond the scope of this study. In any case, an important ingredient is the weakening of the AMOC in subtropical and subpolar latitudes, caused by a decrease in Labrador Sea Water formation as a response to global warming, while the deep-water production in the Nordic Seas is even slightly enhanced. The exact mechanisms of how gyre and overturning circulations interact are also difficult to disentangle. In the historical simulations, changes in AMOC and SPG circulation appear to happen more or less instantaneously, whereas analyses of the unperturbed control simulation suggest that AMOC variations are leading by a few years.

Many CMIP5 models feature a reduction of the AMOC strength already in the 20th century (Drijfhout et al., 2012). A characteristic feature of these simulations is the "warming hole" above the subpolar North Atlantic that can also be identified in observations (e.g. in the HadSST data set; Rayner et al., 2006). A cool surface temperature spot within the intensified SPG is also characteristic for our 20th-century simulations (Fig. 6) and related to the mechanism described above. Drijfhout et al. (2012) decompose the temperature pattern in a radiatively forced and an AMOC fingerprint and conclude that the cold subpolar North Atlantic is indeed related to an AMOC decline. Kim and An (2012) come to a similar conclusion analysing CO_2-doubling experiments from the Coupled Model Intercomparison Project phase 3 database.

Another indication that the mechanism described here is at work in reality comes from palaeoceanographic reconstructions for the late Holocene. Miettinen et al. (2012) compare the temporal evolution of ocean temperatures at two locations, the Voering Plateu in the Norwegian Sea and the SPG region south of the Reykjanes Ridge. They find that low-frequency fluctuations occur out of phase: the Voering Plateau record features, for example, a cold anomaly during the Little Ice Age, whereas the SPG is warmer than normal during this period. Such a behaviour is compatible with the findings described here: a weaker SPG in the LIA (Fig. 3) would feature a less dense and warmer centre (opposite to what is seen for the strong-gyre anomaly in Fig. 6) and would transport less heat to the Nordic Seas. Such out-of-phase anomalies of the barotropic stream function in the SPG region and the Nordic Seas can also be seen in Fig. 4b. A detailed investigation of the variations and processes during the pre-industrial millennium and their relation to natural forcing will be the subject of a subsequent study.

Obtaining a comprehensive view from long-term direct observations of temperature, salinity, or transports remains challenging. There exist only a few long-term time series. Many continuous records, such as those from weather ships (e.g. Østerhus and Gammelsrød, 1999) cover the last decades and are characterized by multidecadal variability. The temperature measurements over the 20th century near Svalbard by Pavlov et al. (2013) and one of the longest time series available at all, namely that of the Kola section in the Barents Sea (e.g. Skagseth et al., 2008), support the pronounced warming in the Atlantic Water branch in the industrial period. Polyakov et al. (2004) synthesized various observational data sets to conclude that the intermediate Atlantic Water layer in the Arctic shows a continuous warming trend that is superposed by multidecal variability. Combining proxy data and observations, Cunningham et al. (2013) compiled a synthesis of SST changes in the north-eastern North Atlantic and the Nordic Seas during the last millennium. For the 20th century (their Fig. 1a), they report that most of the records reflecting the Atlantic Water branch along Scotland and Norway indicate a warming, while other records from the subpolar North Atlantic indicate neutral or cooling conditions. High-resolution proxies from the Iceland Basin (Hall et al., 2010) over the last 230 years indicate cooling of SSTs in the central subpolar gyre region, which would be consistent with our findings. The available SST gridded data sets HadISST (Rayner et al., 2006) and ERSSTv3 (Smith and Reynolds, 2004) as well as the Simple Ocean Data Assimilation (SODA) reanalysis (Carton and Giese, 2008) are all characterized by a cooling trend in the subpolar gyre region (Drijfhout et al., 2012; Kim and An, 2012). Polyakov et al. (2010) have used historical data from the North Atlantic Ocean and decomposed the changes between the 1920s and present into non-linear trend and multidecadal variability patterns. The large-scale non-linear trend pattern resembles the 20th-century SST trend in the HadISST and is characterized by cooling over the subpolar gyre (see their Fig. 5) and warming in the subtropical North Atlantic and on the northwestern European Shelf, again compatible with our results for the 20th-century simulations. On the other hand, the 20th-century compilation of temperature and salinity data from the subpolar gyre region by Reverdin (2010) compares less well with our study: the central SPG at about 60° N is characterized by slightly positive temperature and negative density trends.

Uncertainties in early observations and reconstructions preclude a definite answer to the question of to what degree the findings reported here can be verified by observations. While the dynamical mechanisms proposed here to explain the enhanced heat transfer to the Arctic appear largely compatible with observed features in the North Atlantic, they may depend on the particular model system. Moreover, like many other CMIP5 models, MPI-ESM features large SST and circulation biases in the North Atlantic. In particular, the path of the Gulf Stream/North Atlantic Current is too zonal (Jungclaus et al., 2013), which has direct consequences for the shape of the gyres. This may affect the warm-water path from the subtropics to the Nordic Seas. Using observations and model simulations for the second half of the 20th century, Hátún et al. (2005) concluded that a weaker (and less zonally extended) SPG would allow more warm and saline water to enter the Nordic Seas. Our simulations along with other CMIP5 ESMs (Born et al., 2013a; Koenigk and Bradeau, 2014) and stand-alone ocean model simulations with the same ocean model as used here, but forced by reanalysis data (Müller et al., 2014), suggest that a stronger SPG carries more subtropical AW into the Nordic Seas and the Arctic. This discrepancy may be related to the specific situation of the late 20th century described by Hátún et al. (2005), where SPG changes were mainly related to the atmospheric forcing (Häkkinen and Rhines, 2009; see also Born et al., 2013b).

A 30 TW increase in heat transfer to the Arctic over 100 years as suggested by our simulations for the 20th century is an important contribution to the Arctic heat budget (Serreze et al., 2007). Dividing by the area of the Arctic, it corresponds to a substantial forcing of about $2\,\mathrm{Wm}^{-2}$. Jung-

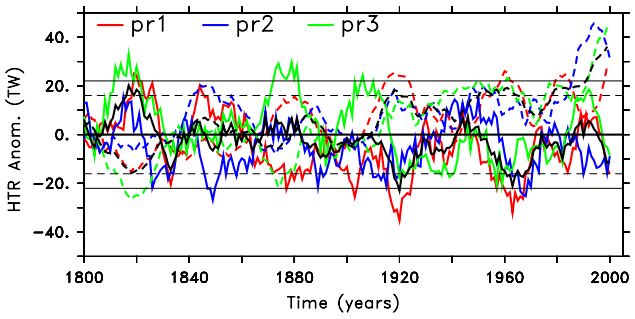

Figure 9. Time series of simulated (solid lines) atmospheric heat transports (AHTR) and (dashed lines) TOHTR at 70° N as anomalies w.r.t. the pre-industrial mean (coloured lines for experiments pr1, pr2, pr3; time series are shown as black dashed and solid lines denote the respective ensemble means). The horizontal black lines bracketing the zero lines are the respective 2σ ranges derived from the PiCtrl experiment. An 11-year running mean was applied to all data sets.

claus and Koenigk (2010) and Beitsch et al. (2014) have shown that multidecadal variations in TOHTR to the Arctic impact the Arctic climate. For positive TOHTR anomalies, the sea-ice cover decreases most pronounced in the Barents Sea and causes considerable variations in ocean–atmosphere heat fluxes. Although only a small fraction of the Arctic is affected, the associated warming leads to positive pan-Arctic temperature anomalies. Moreover, the heat-flux changes affect the atmospheric circulation. An associated feedback mechanism is the Bjerknes compensation (Bjerknes, 1964; Shaffrey and Sutton, 2006; Jungclaus and Koenigk, 2010): on multidecadal timescales, TOHTR and atmospheric heat transports (AHTR, here derived from the components of moist and dry static energy advection following Keith, 1995) are strongly coupled and may compensate each other. Thus, both TOHTR and AHTR need to be considered for an assessment of the lateral heat transfer changes as part of the Arctic heat budget. Comparing TOHTR and AHTR at 70° N (Fig. 9) indicates considerable multidecadal variability, where the respective TOHTR and AHTR tend to evolve out of phase. However, there is no compensation of the strong positive trend in TOHTR during the last decades of the simulation. Therefore we conclude that there is a net positive contribution from the lateral heat fluxes to the Arctic heat budget and to the warming in recent decades. An assessment of all terms of the Arctic heat budget and the feedback mechanisms leading to Arctic Amplification is, however, beyond the scope of our paper. The magnitude of TOHTR changes appears to play a decisive role in the amplitude of pan-Arctic warming, and sea-ice evolution in climate-change simulations (Mahlstein and Knutti, 2011). These authors concluded that the TOHTR changes contribute significantly to Arctic amplification, but they also identified considerable differences in the TOHTR magnitude in the CMIP3 model suite as a cause for model uncertainty in projected Arctic warming.

6 Conclusions

The MPI-ESM last-millennium simulations consistently reproduce enhanced 20th-century warming of AW at the boundary between the Nordic Seas and the Arctic compared with pre-industrial variability. The warming of AW in Fram Strait is an indicator for a prominent ($\sim 40\,\%$) increase in oceanic heat transfer to the Arctic during the 20th century. In the simulations, we are able to trace back the heat transport changes to a re-organization of the large-scale ocean circulation in the subpolar North Atlantic. The SPG and the associated northward heat transport are intensified by the global-warming-induced weakening of the AMOC and changes in the density structure associated with modified deep-water formation. The latter also leads to a slight intensification of the overturning in high northern latitudes. Together, the gyre- and overturning-related heat transport changes lead to an increase in the heat transfer to the Nordic Seas and the Arctic. Changes in wind-stress curl do not appear to be significantly different from the unperturbed variability, but wind-stress changes may nonetheless play a role in triggering the mechanism. Transient simulations over the late Holocene provide a valuable reference frame to discriminate unprecedented changes such as those observed in the 20th century from natural or internal fluctuations.

Acknowledgements. This work was supported by the European Community's 7th Framework Programme (FP7/2007–2013) under the grant agreements no. 308299 (NACLIM) and no. 243908 (Past4Future). D. Z. was supported by the German Federal Ministry for Education and Research (BMBF) Miklip project (FKZ: 01LP1158A). The MPI-ESM-P simulations were conducted at the German Climate Computing Center (DKRZ). The authors thank Chao Li and two anonymous reviewers for comments that helped improve the manuscript.

The service charges for this open access publication have been covered by the Max Planck Society.

Edited by: V. Rath

References

Ahmed, M. and the PAGES 2k Consortium: Continental-scale temperature variability during the last two millennia, Nat. Geosci., 6, 339–346, doi:10.1038/ngeo1797, 2013.

Årthun, M., Eldevik, T., Smedsrud, L. H., Skagseth, Ø., and Ingvaldsen, R. B.: Quantifying the influence of Atlantic heat on Barents Sea ice variability and retreat, J. Climate, 25, 4736–4743, doi:10.1175/JCLI-D-11-00466.1, 2012.

Beitsch, A., Jungclaus, J. H., and Zanchettin, D.: Patterns of decadal-scale Arctic warming events in simulated climate, Clim. Dynam., 43, 1773–1789 doi:10.1007/s00382-013-2004-5, 2014.

Bengtsson, L., Semenov, V. A., and Johannessen, O. M.: The early twentieth-century warming in the Arctic – a possible explanation, J. Climate, 18, 4045–4057, doi:10.1175/1520-0442(2004)017<4045:TETWIT>2.0.CO;2, 2004.

Bjerknes, J.: Atlantic air-sea interaction, Adv. Geophys., 10, 1–82, 1964.

Boessenkool, K. P., Hall, I. R., Elderfield, H., and Yashayaev, I.: North Atlantic climate deep-ocean flow speed changes during the last 230 years, Geophys. Res. Lett., 34, L13614, doi:10.1029/2007GL030285, 2007.

Booth, B. B. B., Dunstone, N. J., Halloran, P. R., Andrews, T., and Bellouin, N.: Aerosols implicated as a prime driver of twentieth century North Atlantic climate variability, Nature, 484, 228–232, doi:10.1038/nature10946, 2012.

Born, A., Stocker, T. F., Raible, C. C., and Levermann, A.: Is the Atlantic subpolar gyre bistable in comprehensive climate models? Clim. Dynam., 40, 2993–3007, doi:10.1007/s00382-012-1525-7, 2013a.

Born, A., Stocker, T. F., and Sandø, A. B.: Coupling of eastern and western subpolar North Atlantic: salt transport in the Irminger Current, Ocean Sci. Discuss., 10, 555–579, doi:10.5194/osd-10-555-2013, 2013b.

Bothe, O., Jungclaus, J. H., and Zanchettin, D.: Consistency of the multi-model CMIP5/PMIP3-past1000 ensemble, Clim. Past, 9, 2471–2487, doi:10.5194/cp-9-2471-2013, 2013.

Carton, J. A. and Giese, B. S.: A reanalysis of ocean climate using Simple Ocean Data Assimilation (SODA), Mon. Weather Rev., 136, 2999–3017, doi:10.1175/2007MWR1978.1, 2008.

Crowley, T. J. and Unterman, M. B.: Technical details concerning development of a 1200 yr proxy index for global volcanism, Earth Syst. Sci. Data, 5, 187–197, doi:10.5194/essd-5-187-2013, 2013.

Cunningham, L., Austin, W. E. N., Knudsen, K. L., Eiriksson, J., Scourse, J. D., Wanamaker Jr., A. D., Butler, P. G., Cage, A. G., Richter, T., Husum, K., Hald, M., Andersson, C., Zorita, E., Linderholm, H. W., Gunnarson, B. E., Sicre, M.-A., Sejruo, H. P., Jiang, H., and Wilson, R.: Reconstructions of surface ocean conditions from the northeast Atlantic and Nordic Seas during the last millennium, The Holocene, 23, 921–935, doi:10.1177/0959683613479677, 2013.

Drijfhout, S. S. and Hazeleger, W.: Changes in MOC and gyre-induced Atlantic Ocean heat transport, Geophys. Res. Lett., 33, L07707, doi:10.1029/2006GL025807, 2006.

Drijfhout, S., van Oldenborgh, G. J., and Cimatoribus, A.: Is a decline of AMOC causing the warming hole above the North Atlantic in observed and modeled warming patterns?, J. Climate, 25, 8373–8379, doi:10.1175/JCLI-D-12-00490.1, 2012.

Dylmer, C. V., Giradeau, J., Eynaud, F., Husum, K., and De Vernal, A.: Northward advection of Atlantic water in the eastern Nordic Seas, Clim. Past, 9, 1505–1518, doi:10.5194/cp-9-1505-2013, 2013.

Eden, C. and Jung, T.: North Atlantic interdecadal variability: oceanic response to the North Atlantic Oscillation (1865–1997), J. Climate, 14, 676–691, 2001.

Fernández-Donado, L., González-Rouco, J. F., Raible, C. C., Ammann, C. M., Barriopedro, D., García-Bustamante, E., Jungclaus, J. H., Lorenz, S. J., Luterbacher, J., Phipps, S. J., Servonnat, J., Swingedouw, D., Tett, S. F. B., Wagner, S., Yiou, P., and Zorita, E.: Large-scale temperature response to external forcing in simulations and reconstructions of the last millennium, Clim. Past, 9, 393–421, doi:10.5194/cp-9-393-2013, 2013.

Giorgetta, M. A., Jungclaus, J. H., Reick, C. H., Legutke, S., Brovkin, V., Crueger, T., Esch, M., Fieg, K., Glushak, K., Gayler, V., Haak, H., Hollweg, H.-D., Ilyina, T., Kinne, S., Kornblueh, L., Matei, D., Mauritsen, T., Mikolajewicz, U., Mueller, W. A., Notz, D., Raddatz, T., Rast, S., Redler, R., Roeckner, E., Schmidt, H., Schnur, R., Segschneider, J., Six, K., Stockhause, M., Wegner, J., Widmann, H., Wieners, K.-H., Claussen, M., Marotzke, J., and Stevens, B.: Climate and carbon cycle changes from 1850 to 2100 in MPI-ESM simulations for the Coupled Model Intercomparison Project phase 5, J. Adv. Model Earth Syst., 5, 1–26, doi:10.1002/jame.20038, 2013.

Greatbatch, R., Fanning, A., Goulding, A., and Levitus, S.: A diagnosis of interpentadal circulation changes in the North Atlantic, J. Geophys. Res., 96, 22009–22023, 1991.

Häkkinen, S. and Rhines, P. B.: Shifting surface currents in the northern North Atlantic, J. Geophys. Res., 114, C04005, doi:10.1029/2008JC004883, 2009.

Hald, M., Salomonsen, G. R., Husum, K., and Wilson, L. J.: A 2000 year record of Atlantic Water temperature variability from Malangen Fjord, northeastern North Atlantic, The Holocene, 21, 1049–1059, doi:10.1177/0959683611400457, 2011.

Hall, I. R., Boessenkool, K. P., Barker, S., McCave, N., and Elderfield, H.: Surface and deep ocean coupling in the subpolar North Atlantic during the last 230 years, Paleoceanography, 25, PA2101, doi:10.1029/2009PA001886, 2010.

Hátún, H., Sandø, A. B., Drange, H., Hansen, B., and Valdimarsson, H.: Influence of the Atlantic subpolar gyre on the thermohaline circulation, Science, 309, 1841–1844, doi:10.1126/science.1114777, 2005.

Jungclaus, J. H. and Koenigk, T.: Low-frequency variability of the Arctic climate: the role of oceanic and atmospheric heat transport variations, Clim. Dynam., 34, 265–279, doi:10.1007/s00382-009-0569-9, 2010.

Jungclaus, J. H., Haak, H., Mikolajewicz, U., and Latif, M.: Arctic-North Atlantic interactions and multidecadal variability of the meridional overturning circulation, J. Climate, 18, 4016–4034, 2005.

Jungclaus, J. H., Macrander, A., and Käse, R. H.: Modelling the overflow across the Greenland-Scotland Ridge, in: Arctic-subarctic ocean fluxes, edited by: Dickson, R. R., Meincke, J., and Rhines, P., Springer, Dordrecht, 527–549, 2008.

Jungclaus, J. H., Lorenz, S. J., Timmreck, C., Reick, C. H., Brovkin, V., Six, K., Segschneider, J., Giorgetta, M. A., Crowley, T. J., Pongratz, J., Krivova, N. A., Vieira, L. E., Solanki, S. K., Klocke, D., Botzet, M., Esch, M., Gayler, V., Haak, H., Raddatz, T. J., Roeckner, E., Schnur, R., Widmann, H., Claussen, M., Stevens, B., and Marotzke, J.: Climate and carbon-cycle variability over the last millennium, Clim. Past, 6, 723–737, doi:10.5194/cp-6-723-2010, 2010.

Jungclaus, J. H., Fischer, N., Haak, H., Lohmann, K., Marotzke, J., Matei, D., Mikolajewicz, U., Notz, D., and von Storch, J.-S.: Characteristics of the ocean simulations in the Max Planck Institute Ocean Model (MPIOM) the ocean component of the

MPI-Earth system model, J. Adv. Model Earth Syst., 5, 422–446, doi:10.1002/jame.20023, 2013.

Kaufman, D. S., Schneider, D. P., McKay, N. P., Ammann, C. M., Bradley, R. S., Briffa, K. R., Miller, G. H., Otto-Bliesner, B. L., Overpeck, J. T., Vinther, B. M., and Arctic Lakes 2K project members: Recent warming reverses long-term Arctic cooling, Science, 325, 1236–1239, doi:10.1126/science.1173983, 2009.

Keith, D. W.: Meridional energy transport: uncertainty in zonal means, Tellus, 47A, 30–44, 1995.

Kim, H. and An, S.-I.: On the subarctic North Atlantic cooling due to global warming, Theor. Appl. Climatol., 114, 1–19, doi:10.1007/s00704-012-0805-9, 2012.

Kinnard, C., Zdanowicz, C. M., Fisher, D. A., Isaksson, E., De Vernal, A., and Thompson, L. G.: Reconstructed changes in Arctic sea ice over the last 1,450 years, Nature, 479, 509–513, doi:10.1038/nature10581, 2011.

Koenigk, T. and Brodeau, L.: Ocean heat transport into the Arctic in the twentieth and twenty-first century in EC-Earth, Clim. Dynam., 42, 3101–3120, doi:10.1007/s00382-013-1821-x,2014.

Latif, M., Böning, C., Willebrand, J., Biastoch, A., Dengg, J., Keenlyside, N., Schweckendiek, U., and Madec, G.: Is the Thermohaline Circulation Changing?, J. Climate, 19, 4631–4637, doi:10.1175/JCLI3876.1, 2006.

Levermann, A. and Born, A.: Bistability of the Atlantic subpolar gyre in a coarse-resolution climate model, Geophys. Res. Lett., 34, L24605, doi:10.1029/2007GL031732, 2007.

Lohmann, K., Jungclaus, J. H., Matei, D., Mignot, J., Menary, M., Langehaug, H. R., Ba, J., Gao, Y., Otterå, O. H., Park, W., and Lorenz, S.: The role of subpolar deep water formation and Nordic Seas overflows in simulated multidecadal variability of the Atlantic meridional overturning circulation, Ocean Sci., 10, 227–241, doi:10.5194/os-10-227-2014, 2014.

Lozier, M. S.: Deconstructing the Conveyor Belt, Science, 328, 1507–1511, doi:10.1126/science.1189250, 2010.

Lozier, M. S., Roussenov, V., Reed, M. S. C., and Williams, R. G.: Opposing decadal changes for the North Atlantic meridional overturning circulation, Nat. Geosci., 3, 728–734, doi:10.1038/NGEO947, 2010.

Mahlstein, I. and Knutti, R.: Ocean heat transport as a cause for model uncertainty in projected Arctic warming, J. Climate, 24, 1451–1460, doi:10.1175/JCLI3713.1, 2011.

Marsland, S. J., Haak, H., Jungclaus, J. H., Latif, M., and Roeske, F.: The Max-Planck-Institute global ocean/sea-ice model with orthogonal curvilinear coordinates, Ocean Model., 5, 91–127, 2003.

Miettinen, A., Divine, D., Koç, N., Godtliebsen, F., and Hall, I. R.: Multicentennial variability of the sea surface temperature gradient across the subpolar North Atlantic over the last 2.8kyr, J. Climate, 25, 4205–4219, doi:10.1175/JCLI-D-11-00581.1, 2012.

Müller, W. A., Matei, D., Bersch, M., Jungclaus, J. H., Haak, H., Lohmann, K., Compo, G. P., Sardeshmukh, P. D., and Marotzke, J.: A 20th century reanalysis-forced ocean model to reconstruct the North Atlantic climate variations during the 1920s, Clim. Dynam., doi:10.1007/s00382-014-2267-5, in press, 2014.

Østerhus, S. and Gammelsrød, T.: The abyss of the Nordic Seas is warming, J. Climate, 12, 3297–3304, 1999.

Pavlov, A., Tverberg, V., Ivanov, B., Nilsen, F., Falk-Petersen, S., and Granskog, M.: Warming of Atlantic Water in two west Spitsbergen fjords over the last century (1912–2009), Polar Res., 32, 11206, doi:10.3402/polar.v32i0.11206, 2013.

Polyakov, I. V., Alekseev, G. V., Timokhov, L. A., Bhatt, U. S., Colony, R. L., Simmons, H. L., Walsh, D., Walsh, J. E., and Zakharov, V. F.: Variability of the Intermediate Atlantic Water of the Arctic Ocean over the last 100 years, J. Climate, 17, 4485–4497, 2004.

Polyakov, I. V., Alexeev, V. A., Bhatt, U. S., Polyakova, E. I., and Zhang, X.: North Atlantic warming: patterns of long-term trend and multidecadal variability, Clim. Dynam., 34, 439–457, doi:10.1007/s00382-008-0522-3, 2010.

Pongratz, J., Reick, C. H., Raddatz, T., and Claussen, M.: A reconstruction of global agricultural areas and land cover for the last millennium, Global Biogeochem. Cy., 22, GB3018, doi:10.1029/2007GB003153, 2008.

Rayner, N. A., Brohan, P., Parker, D. E., Folland, C. K., Kennedy, J. J., Vanicek, M., Ansell, T. J., and Tett, S. F. B.: Improved analyses of changes and uncertainties in sea surface temperature measured in situ since the mid nineteenth century: the HadSST2 data set, J. Climate, 19, 446–469, doi:10.1175/jcli3637.1, 2006.

Reverdin, G.: North Atlantic Subpolar Gyre Surface Variability (1895–2009), J. Climate, 23, 4571–4584, doi:10.1175/2010JCLI3493.1, 2010.

Saenko, O. A., Fyfe, J. C., and England, M. H.: On the response of the oceanic wind-driven circulation to atmospheric CO_2 increase, Clim. Dynam., 25, 415–426, doi:10.1007/s00382-005-0032-5, 2005.

Schauer, U., Beszynnka-Möller, A., Walczowski, W., Fahrbach, E., Piechura, J., and Hansen, E.: Variations of measured heat flow through Fram Strait between 1997 and 2006, in: Arctic-subarctic ocean fluxes, edited by: Dickson, R. R., Meincke, J., and Rhines, P., Springer, Dordrecht, 65–85, 2008.

Schmidt, G. A., Jungclaus, J. H., Ammann, C. M., Bard, E., Braconnot, P., Crowley, T. J., Delaygue, G., Joos, F., Krivova, N. A., Muscheler, R., Otto-Bliesner, B. L., Pongratz, J., Shindell, D. T., Solanki, S. K., Steinhilber, F., and Vieira, L. E. A.: Climate forcing reconstructions for use in PMIP simulations of the last millennium (v.1.0), Geosci. Model Dev., 4, 33–45, doi:10.5194/gmd-4-33-2011, 2011.

Sedláček, J. and Mysak, L. A.: A model study of the Little Ice Age and beyond: changes in ocean heat content, hydrography and circulation since 1500, Clim. Dynam., 33, 461–475, doi:10.1007/s00382-008-0503-6, 2009.

Serreze, M. C., Barnett, A. P., Slater, A. G., Steele, M., Zhang, J., and Trenberth, K. E.: The large-scale energy budget of the Arctic, J. Geophys. Res., 112, D11122, doi:10.1029/2006JD008230, 2007.

Shaffrey, L. and Sutton, R.: Bjerknes compensation and the decadal variability of the energy transports in a coupled climate model, J. Climate, 19, 1167–1448, doi:10.1175/JCLI3652.1, 2006.

Shi, F., Yang, B., Ljungqvist, F. C., and Yang, F.: Multi-proxy reconstruction of Arctic summer temperatures over the past 1400 years, Clim. Res., 54, 113–128, doi:10.3354/cr01112, 2012.

Skagseth, Ø., Furevik, T., Ingvaldsen, R., Loeng, H., Mork, K. A., Orvik, K. A., and Ozhigin, V.: Volume and heat transport to the Arctic Ocean via the Norwegian and Barents Sea, in: Arctic-subarctic ocean fluxes, edited by: Dickson, R. R., Meincke, J., and Rhines, P., Springer, Dordrecht, 45–64, 2008.

Smith, T. M. and Reynolds, R. W.: Improved extended reconstruction of SST (1854–1997), J. Climate, 17, 2466–2477, doi:10.1175/1520-0442(2004)017<2466:IEROS>2.0.CO;2, 2004.

Spielhagen, R. F., Wagner, K., Sørensen, S. A., Zamelczyk, K., Kandiano, E., Budeus, G., Husum, K., Marchitto, T. M., and Hald, M.: Enhanced modern heat transfer to the Arctic by warm Atlantic Water, Science, 331, 450–453, doi:10.1126/science.1197397, 2011.

Stevens, B., Giorgetta, M., Esch, M., Mauritsen, T., Crueger, T., Rast, S., Salzmann, M., Schmidt, H., Bader, J., Block, K., Brokopf, R., Fast, I., Kinne, S., Kornblueh, L., Lohmann, U., Pincus, R., Reichler, T., and Roeckner, E.: Atmosphereric component of the MPI-M Earth system Model: Echam6, J. Adv. Model Earth Syst., 5, 146–172, doi:10.1002/jame.20015, 2013.

Vieira, L. E. A., Solanki, S. K., Krivova, N. A., and Usoskin, I.: Evolution of the solar irradiance during the Holcene, Astron. Astroph., 531, A6, doi:10.1051/0004-6361/201015843, 2011.

Wang, Y.-M., Lean, J. L., and Sheeley Jr., N. R.: Modeling the Sun's magnetic field and irradiance since 1713, Astrophys. J., 625, 522–538, doi:10.1086/429689, 2005.

Werner, K., Spielhagen, R. F., Bauch, D., Hass, H. C., Kandiano, E., and Zamelcyk, K.: Atlantic water advection to the eastern Fram Strait – multiproxy evidence for late Holocene variability, Paleogeography, Paleoclimatology, Paleoecology, 308, 264–276, doi:10.1016/j.palaeo.2011.05.030, 2011.

Zanchettin, D., Timmreck, C., Graf, H.-F., Rubino, A., Lorenz, S., Lohmann, K., Krüger, K., and Jungclaus, J. H.: Bi-decadal variability excited in the coupled ocean-atmosphere system by strong tropical volcanic eruptions, Clim. Dynam., 39, 419–444, doi:10.1007/s00382-011-1167-1, 2012.

Zanchettin, D., Timmreck, C., Bothe, O., Lorenz, S. J., Hegerl, G., Graf, H.-F., Luterbacher, J., and Jungclaus, J. H.: Background conditions influence the decadal climate response to strong volcanic eruptions, J. Geophys. Res.-Atmos., 118, 4090–4106, doi:10.1002/jgrd.50229, 2013.

Zhang, R., Delworth, T. L., Sutton, R., Hodson, D. L. R., Dixon, K. W., Held, I. M., Kushnir, Y., Marshall, J., Ming, Y., Msadek, R., Robson, J., Rosati, A. J., Ting, M. F., and Vecci, G.: Have aerosols caused the observed Atlantic multidecadal variability?, J. Atmos. Sci., 70, 1135–1144, doi:10.1175/JAS-D-12-0331.1, 2013.